

BENCHMARK MEASUREMENT OF IODOBENZENE ION FRAGMENTATION RATES

J. DANNACHER *, H.M. ROSENSTOCK, R. BUFF **, A.C. PARR, R.L. STOCKBAUER
National Measurement Laboratory, National Bureau of Standards, Washington, DC 20234, USA

and

R. BOMBACH and J.-P. STADELMANN
Physikalisch Chemisches Institut der Universität Basel, Klingelbergstrasse 80, CH-4056 Basel, Switzerland

Received 5 March 1982; in final form 10 January 1983

The unimolecular fragmentation rate of iodobenzene ion has been studied by variable residence time photoelectron–photoion coincidence techniques. The techniques employed variable wavelength with threshold photoelectron detection and fixed (58.4 nm) wavelength with variable energy photoelectron detection, respectively. Residence times of 1.0 ± 0.25 or 5.9 ± 0.3 and 21 ± 1 or $57 \pm 1 \mu\text{s}$ were employed. The four sets of measurements were independently analyzed using exact counting of harmonic oscillator states, taking into account the appropriate (and different) apparatus functions and the thermal energy distributions of the parent ions. The resulting rate-energy dependences and fragmentation threshold values were in excellent agreement with one another. The best-fit rate-energy dependence is proposed as a benchmark for calibration of future rate-energy measurements. The resulting $\Delta H_{\text{IP}}^0(\text{C}_6\text{H}_5^+) = 1133 \pm 5 \text{ kJ mol}^{-1}$ is in excellent agreement with earlier results based on a somewhat simpler method of analysis of chlorobenzene and bromobenzene fragmentation rates. Some remaining uncertainties regarding the transition-state model are discussed.

1. Introduction

Photoelectron–photoion coincidence mass spectrometry is one of the most valuable tools for the study of the dynamic behavior of excited molecular ions. Areas of application include the determination of breakdown curves, the partition of excess energy in ion fragmentation processes, and the determination of the dependence of the unimolecular fragmentation rates on the excitation energy of the fragmenting ion [1]. Prior to or in parallel with these experiments, other experimental approaches have been developed which although less directly, lead to the

same type of information. These include the study of metastable transitions to obtain information on kinetic energy release [2], and the application of first-derivative photoionization [3] or second-derivative electron-impact techniques to give breakdown curves or the energy dependence of fragmentation rates [4]. The successful application of these techniques requires a detailed understanding of and accounting for both the apparatus function and the details of the molecular ionization–fragmentation process. Inevitably some simplifications are made in order to make interpretation of the raw data tractable. In a number of instances the same system has been studied by several techniques or variants of one technique, and the ensuing comparison of final results often raises serious questions and stimulates corrections and refinements in the methodology. Such comparisons have recently been made for the measurement of fragment kinetic energies in metastable transitions [2], and for the determination of breakdown

* Guest worker, NBS, permanent address: Physikalisch Chemisches Institut der Universität Basel, Klingelbergstrasse 80, CH-4056 Basel, Switzerland.

** Intergovernmental Personnel Act Appointee at the National Bureau of Standards 1980–1982, permanent address: Department of Physics and Astronomy, University of Alabama, University, Alabama 35486, USA.

curves for fragmentation branching ratios by various coincidence techniques [5–8]. In addition, data have been obtained by several methods for the energy dependence of kinetic energy release in fragmentation of methyl iodide ion [9–11]. These warrant further scrutiny, since there is disagreement among the results.

The present study is concerned with the determination of the rate-energy dependence of iodobenzene cation fragmentation. Comparison of the rather limited body of information on determination of rate-energy curves of large molecules [12–19] reveals diverse patterns of accord and disagreement among different techniques for different molecules. We have chosen iodobenzene because of the large diversity of techniques for determining the rate-energy dependence which have been and can be applied, thus affording a rather broad area of comparison of techniques and interpretations.

The fragmentation of photoionized iodobenzene was first studied by Vilesov [20]. A few years later Baer et al. [12] published rate-energy data for iodobenzene cation, which had been inferred from the $C_6H_5^+$ fragment ion time-of-flight distribution as obtained in coincidence experiments. More recently Pratt and Chupka [19] reported results on three halobenzenes including iodobenzene, based on kinetic analysis of the first derivative of the photoionization yield curve of the metastable transition for loss of halogen atoms. In the present work three photoelectron–photoion coincidence spectrometers were used. The NBS instrument (I) employs variable wavelength photoionization with detection of threshold electrons and time-of-flight mass analysis. The two instruments at Basel (II and III) use helium ($I\alpha$) resonance radiation with variable electron energy analysis, and mass analysis by means of time-of-flight only (II) or in combination with a quadrupole mass spectrometer (III).

The experimentally accessible range of fragmentation rates depends on the type of apparatus used. The values of the rate constant for the dissociation of iodobenzene cation reported by Baer et al. [12], lie between 9×10^4 and $2.4 \times 10^6 \text{ s}^{-1}$. The photoionization technique of Pratt and Chupka [19] is sensitive to rates between 10^4 and 10^5 s^{-1} and yields one value and a slope at a single excitation energy. The value is $4.2 \times 10^4 \text{ s}^{-1}$ at 11.52 eV in the case of

iodobenzene cation. Referring to the sampling times used (see text) and an energy span where the fraction of iodobenzene molecular ions decreases from 95 to 5%, the NBS apparatus allowed the measurement of rates between 10^4 and $3 \times 10^6 \text{ s}^{-1}$. The corresponding range of the Basel instruments would be 10^3 to $1.5 \times 10^5 \text{ s}^{-1}$. However, as a consequence of the very low Franck–Condon factor in the threshold region of the investigated dissociation reaction this range is reduced to 10^4 to $1.5 \times 10^5 \text{ s}^{-1}$ in the present case. A significant difference between the NBS and Basel instruments is that the former, operating in the threshold electron detection mode, will sample ions produced by autoionization as well as direct ionization. The Basel instruments, using helium resonance radiation and selection of a narrow band of high energy ($\approx 10 \text{ eV}$) photoelectrons will only sample ions produced by direct ionization.

2. Experimental

The NBS threshold electron–ion coincidence apparatus has been described in detail elsewhere [5,13,14,21]. By varying the delay of the ion drawout pulse, it is possible to determine the wavelength dependence of the extent of ion fragmentation at different ion source residence times. Two such times, $1.00 \pm 0.25 \mu\text{s}$ and $5.9 \pm 0.3 \mu\text{s}$ were used in this study. The coincidence time-of-flight spectra can be partitioned into three sections which contain a smaller or larger fraction of the totally detected events, depending on the value of the selected photon energy and the sampling time used. There are relatively narrow peaks centered around the expected parent and daughter ion flight times due to undissociated molecular ions and fragments produced by rapid ($k \geq 5 \times 10^6 \text{ s}^{-1}$) decays, respectively. Moreover, there is a continuous distribution of events in between these two peaks arising from ion dissociation in the accelerating–focusing region, i.e. corresponding to slow fragmentation processes relative to the time scale of the experiment. All ions in this intermediate region were included in the parent ion abundance. Fragment ions were thus defined as those ions formed essentially prior to the application of the ejection pulse [5,13,14]. The apparatus had an effective threshold electron energy resolution (including

photon bandwidth) of ≈ 30 meV fwhm [5], and an ion collection efficiency of 10–20%.

The Basel fixed wavelength experiments employed two instruments. The earlier model consisted of a simple time-of-flight mass analyzer and a hemispherical electron energy analyzer which selected a narrow band of energetic photoelectrons produced by He-I α irradiation of the sample gas. This instrument has been described in detail elsewhere [22]. The more recent instrument [23] consists of the same hemispherical electron energy analyzer combined with a quadrupole mass analyzer which had been employed in an earlier apparatus [6]. Both fixed wavelength instruments had an ion transmission coefficient of $\approx 25\%$, and the electron energy sampling function was essentially a gaussian curve with 80 meV fwhm. The electron collection efficiency was $\approx 0.1\%$ for the earlier instrument (II) and $\approx 0.5\%$ for the later one (III). The relevant time scales of these two experiments are defined in such a way that molecular ions which do not decay within $21 \pm 1 \mu\text{s}$ (II) and $57 \pm 1 \mu\text{s}$ (III), respectively, are termed parent ions.

3. Results and discussion

3.1. PES, TPES, PI-MS

The He-I α photoelectron spectrum (PES) and the threshold photoelectron spectrum (TPES) of iodobenzene between the onset and 12 eV are presented in fig. 1. The spectra were recorded under coincidence conditions. The photoelectron spectra of the halobenzenes have been the topic of numerous experimental and theoretical studies [25,26], and many details of interpretation are still open questions. All that is needed for the present purposes is the assignment given in table 1, which is in accord with most of the earlier literature. The few band systems 1–4 (cf. fig. 1) are essentially associated with the removal of an electron from a b_{1g} - (ring – I, π) (1), an a_{2g} - (the other component of the benzene $1e_{1g}$ orbital which cannot interact with I) (low-energy part of band 2), a b_{2g} - (in-plane lone pair of I) (high-energy part of band 2), a b_{1g} - (out-of-plane lone pair of I) (band 3) and an a_{1g} orbital (ring – I, σ) (band 4). The higher resolution TPES clearly shows some fine structure in the onset region of the spectrum with an aver-

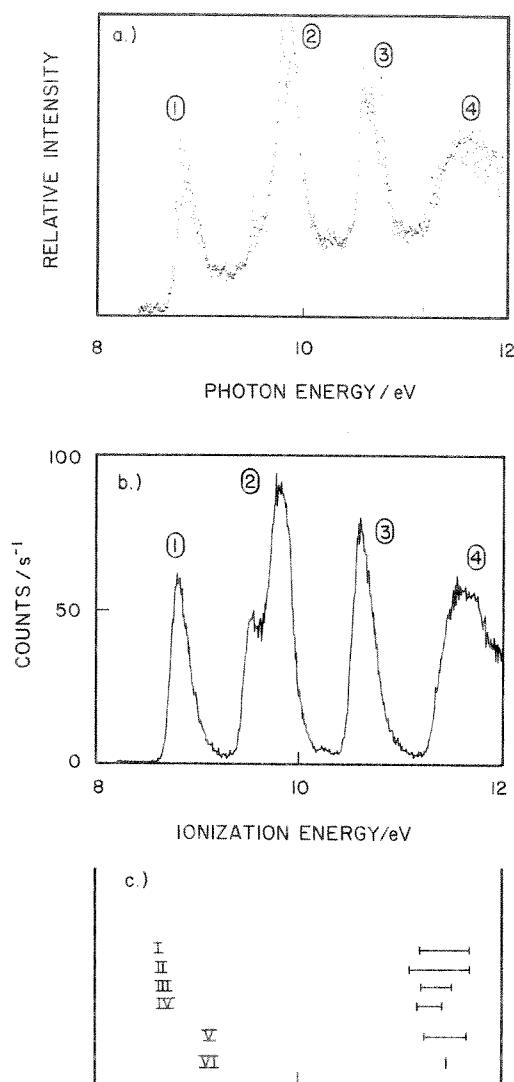


Fig. 1. Threshold-(TPES) (a) and He-I α -(PES) (b) photoelectron spectrum between 8 and 12 eV, as obtained under coincidence conditions. (c) Pertinent energy ranges for this work (data sets I–IV) and the earlier data of Baer et al. (V). VI reflects the energy corresponding to the photoionization results of Pratt and Chupka.

age spacing of ≈ 5 meV. This is ascribed to a normal mode corresponding to the $266 \text{ cm}^{-1}(\text{t})$ mode of neutral iodobenzene as given in ref. [27]. The vibrational fine structure becomes more complicated at higher ionization energy indicating the simultaneous excitation of other modes. An onset energy of 8.685 eV was observed in the highly resolved TPES

Table 1
Photoelectron data for the lowest electronic states of iodobenzene

Band	State	Ionization energy ^{a)}		
		b)	c)	d)
1	\tilde{X}^2B_1	8.792	8.78	8.801
		8.685 ^{e)}	8.60 ^{e)}	8.766 ^{f)}
2	\tilde{A}^2A_2	9.512	9.53	9.52
	\tilde{B}^2B_2	9.775 ^{e)}	9.76	9.77
3	\tilde{C}^2B_1	10.585	10.59	10.563
4	\tilde{D}^2A_1	≈ 11.2 ^{e)}	≈ 11.2 ^{e)}	11.70

a) Corresponding to band maxima.

b) This work, threshold photoelectron spectrum.

c) This work, low-resolution He-I α photoelectron spectrum.

d) Ref. [26]. ^{e)} Band onset.

f) Adiabatic ionization energy given in ref. [16].

spectrum, in good agreement with most literature values and our low-resolution PES spectrum. This value was used as the adiabatic ionization potential, although it might be distorted by hot band effects as suggested in ref. [26]. The ground-state vertical ionization potential observed in the TPES was 8.792 eV. From fig. 1 it is seen that despite the higher energy resolution of the TPES apparatus, the valleys between the bands are not as deep as in the lower resolution PES spectrum. This clearly indicates that there is some contribution from autoionization processes producing some zero kinetic energy electrons.

The He-I α photoionization mass spectrum was also determined. The relative intensities observed for the parent and the various fragment ions are given in

Table 2
He-I α (21.22 eV) photoionization mass spectrum of iodobenzene

Ion	m/z	Relative intensity
$C_6H_5I^+$	204	0.42
$C_6H_5^+$	77	1.00
$C_6H_4^+$	76	0.04
$C_4H_3^+$	51	0.22
$C_4H_2^+$	50	0.04
$C_3H_3^+$	39	0.01
$C_2H_4^+$	28	<0.001
$C_2H_3^+$	27	<0.001

table 2. No iodine-containing fragment ions are observed and, consequently, there are no parent ion hydrogen loss processes to take into account.

3.2. Precision of the measurements

The measurable data that we ultimately wish to analyze are the breakdown curves, i.e. the fraction, f , of parent ions fragmenting within a given residence time period, as a function of the photon energy (NBS apparatus), or the difference between the He-I α (21.21 eV) energy and the nominal acceptance energy of the electron energy analyzer (Basel apparatus). At this point it is appropriate to briefly discuss the precision of these data.

In the NBS apparatus, which operates in the delayed coincidence time-of-flight mode, the signal recorded in a particular channel consists of three distinct components: the genuine signal, a contribution from random coincidences, and a true coincidence signal corresponding to the ion mass in question but arising from ionization by photons of wavelength outside the monochromator band pass (i.e. scattered light). The magnitude of the random coincidence signal is easily assessed and can be corrected for from known information on the total count rates at the electron and ion detector. It is evident that it is strongly dependent on the total collection efficiency for both electrons and ions and on the number of ionization events produced. Further, with the count rates and total counting times feasible in the experiments there is a purely random error depending on the total number of counts in the group of channels defined as fragment, and the rest defined as parent. The total effect of these factors leads to an absolute uncertainty of typically ± 0.01 in the fraction f of parents producing fragments. The effect of scattered light manifests itself most clearly in the fact that some fragment coincidences are already observed at relatively low photon energies and some parent coincidences still at relatively high energies. It is extremely difficult to establish any quantitative details of this correction when one is dealing with a hydrogen many-line light source and it is necessary to make measurements at different wavelength settings. The only palliative is to choose a reasonably intense line near the desired wavelength. With this tactic one still finds some "fragment ions" at low energies and "parent

ions" at high energies. The final tactic employed was to renormalize the data slightly by setting the baseline to zero when the total number of counts in the low-energy fragment or high-energy parent region equalled the magnitude of the statistical counting error. We estimate that this introduces an additional absolute uncertainty of ± 0.01 in f . We note further that any major or unusual wavelength-dependent effects of scattered light would reveal themselves in the form of the corrected breakdown curves obtained in the manner described.

The factors affecting the precision of the corresponding measurements on the Basel instruments are of exactly the same nature but of substantially different relative importance.

It will be recalled that the Basel instruments sample fragmentation rates of somewhat lower magnitude. As will be shown later, this places the corresponding ionization events near the onset and into the steeply rising section of the fourth photoelectron band. Thus part of the data is degraded by the presence of an especially small photoelectron count rate and a correspondingly small fraction of parent ions arising from the ionization events selected for data taking. Fortunately these factors can be evaluated statistically. Further, the overall electron detection efficiency of these instruments is substantially lower than that of the NBS instrument, necessitating operation at higher count rates and requiring larger corrections for random coincidences. In fact, it was only possible to take data at 11.20 eV on the newer apparatus, owing to its larger electron collection efficiency.

The so-called scattered light problem is quite different in character. In addition to the He-I α resonance line, the light source also emits at most 0.5% He-I β radiation which is ≈ 2 eV higher in energy, and also emits still smaller amounts of some higher-energy lines. This is presumably constant in the experiments. At any given electron sampling energy there is thus a small contribution from events produced by ions of ≈ 2 eV higher excitation energy. Neglecting a probably minor difference in the photoionization cross section the relative contribution from these events can be estimated from the relative intensities in the photoelectron spectrum at the nominal ionization energies of $(21.22 - E_{\text{kin,eI}})$ eV and of $(23.09 - E_{\text{kin,eI}})$ eV. Clearly this contribution changes as a function of $E_{\text{kin,eI}}$. However, the present fixed wavelength coin-

idence data on iodobenzene cation are not subject to these effects, since the ionization events due to He-I β radiation produce exclusively fragment ions and the normalization of the data relies only on the fraction of surviving molecular ions as outlined below.

The transmission coefficient for molecular ions is a constant, since their thermal kinetic energy distribution is independent of their internal energy. In He-I α photoelectron-photoion coincidence spectroscopy this constant can be determined accurately at any ionization energy where the generated molecular ions cannot fragment for energetic reasons and, thus, the parent ion branching ratio is by necessity equal to unity. Once this transmission coefficient has been evaluated, the fraction of molecular ions producing fragments can be determined unambiguously at all ionization energies where states of the parent cation are populated on He-I α photoionization. Therefore, as long as only fragment ions of a single mass to charge ratio are formed the molecular as well as this fragment ion breakdown curve are known precisely.

We assess the likely total error in the fraction f of parent ions fragmenting to be ± 0.02 in absolute magnitude, essentially equal to that of the NBS experiments. Exceptions are the rather imprecise data points at 11.20 eV and 11.25 eV corresponding to sampling very near the onset of the fourth photoelectron band (cf. figs. 1 and 2).

An additional contrast between the NBS and Basel experiments is the accuracy of the nominal energy scale. In the threshold photoelectron experiments this is determined principally by the photon monochromator and can be assessed as less than ± 5 meV. Even with careful calibration procedures the locally inhomogeneous potentials and the broader electron energy sampling function limit this accuracy to about ± 10 meV in the He-I α coincidence experiments.

3.3. Definition and accuracy of the sampling time

In order to deduce rate energy functions from the measured breakdown curves the sampling time t of the experiment has to be determined as well. Any inaccuracies in this time estimate will also affect the precision of the rate-energy determination. Dissociations occurring before time t has elapsed lead to the detection of fragment ions. Molecular ions fragment-

ing after t seconds or not at all are termed parent ions. As evidenced by the observed *distributions* of ion flight times, this time t is not sharply defined and subject to all initial conditions, which are mapped into this time-of-flight distribution. A rather good estimate for the average value of t and the errors involved can nevertheless be obtained [14].

The NBS spectrometer operates in a pulsed mode. The effective ion source residence time t is given in first approximation by the time difference between occurrence of the ionization event and the application of the drawout pulse. This time difference has a lower limit of $0.7 \mu\text{s}$ determined by the response of the apparatus and an upper limit determined somewhat variably by the requirement that no significant ion losses occur as a result of escape due to the initial thermal velocity of the parent ions. In addition there is a small time interval, after start of acceleration, within which parents can form fragments with total travel times very close to those of fragments formed before start of ejection. A detailed analysis of this situation [14] leads to an estimate of an additional $0.3 \mu\text{s}$ to define the minimum effective residence time. With these constraints, effective residence times of $1.0 \pm 0.25 \mu\text{s}$ (data set I) and $5.9 \pm 0.3 \mu\text{s}$ (data set II) were chosen for the acquisition of data.

The time scale for data set III, obtained on the first Basel apparatus, is based on a variety of calibration measurements, leading to $t = 21 \pm 1 \mu\text{s}$ in the case of iodobenzene. This value for t reflects the time required to reach the entrance aperture of the drift tube. The later version of this apparatus used to measure data set IV offers an accessible time-range from ≈ 60 to $200 \mu\text{s}$ for an ion of $m/e \approx 200$. This can be achieved by adjusting the axial pass energy of the photoions in the quadrupole mass filter. The minimum time is limited by mass resolution requirements. On the other hand, there is also an upper limit for t , since the ions cannot be retarded arbitrarily long if a high ion collection efficiency is to be maintained. Considering the estimated time dependence of the cross-over energy (see below) and the practically vanishing Franck–Condon factor below 11.2 eV , we chose the longest possible time of $57 \mu\text{s}$ with a standard error of $\pm 1 \mu\text{s}$.

3.4. Basic consequences of the relationship between $k(E^*)$ and f

Assuming quasi-equilibrium behavior of the excited parent cations, the unimolecular fragmentation rate constant $k(E^*)$ is a function only of the totally available excitation energy E^* and the decay can be characterized by

$$I_t(E^*) = I_0(E^*) \exp[-k(E^*)t],$$

where I_0 and I_t denote the number of ions initially generated and those which have survived a time t . Recalling the earlier definition of the fraction of fragment ions formed within time t we have then, in obvious notation

$$k(E^*) = -[\ln(1 - f_t)]/t = -[\ln(p_t)]/t.$$

In the actual experiment the excitation energy is not sharply defined, in part because of the finite resolution of the threshold energy or finite electron energy analyzer. In addition, the sample molecules possess a thermal distribution of vibrational and rotational energy, which must be folded into the photoionization energy distribution sampled by either of the electron energy analyzers. Thus at any nominal energy setting of the apparatus one is sampling a distribution of total excitation energies and, consequently, a distribution of unimolecular rate constants [5]. The effect of this distribution will be considered later. For the present we ignore this smearing and consider the propagation of errors in the parent ion fraction p_t and in the residence time t on $k(E^*)$. Since p_t and t are independent we have for the standard error of the rate constant, $\text{SE}(k)$

$$\text{SE}(k) = \frac{1}{t} \left[\left(\frac{\text{SE}(t) \ln p_t}{t} \right)^2 + \left(\frac{\text{SE}(p_t)}{p_t} \right)^2 \right]^{1/2}.$$

This is only approximately true because of the smearing effects, but it will provide a semiquantitative guide to the precision that may be expected. The estimated uncertainty of any given measured parent fraction and any given residence time in these experiments is such that the standard error of the averaged rate corresponding to such a datum is in the range of 10–20%.

3.5. Analysis of the data

The method of data analysis used in the present work was far more searching than that employed in our earlier studies [5,13,14,16,18] and it is useful to briefly review the earlier methodology.

In the earlier studies two breakdown curves were measured at different residence times. A long residence time cross-over energy and a short-time cross-over shift were established from the data by smoothed linear interpolation. Then it was sought to fit these two experimental parameters by calculating rate-energy curves from quasi-equilibrium theory with various activation energies (i.e. energy thresholds, *not* Arrhenius activation energies) and various sets of transition-state parameters. The latter parameters could be conveniently described by a single quantity, the equivalent activation entropy at 1000 K for the corresponding thermal unimolecular reaction. This led to a useful two-parameter description of the QET model corresponding in a definite but indirect way to the two parameters derived from the actual measured data. The transition-state models were limited to harmonic oscillators, and smoothed densities of state and integrated densities of state were computed using numerical Laplace transform methods. The latter are sufficiently accurate even just above (0.05 eV) threshold. The crucial point to note is that the method utilizes essentially the minimum amount of information contained in the experimental data to obtain an answer. Nevertheless, and pleasingly so, the entire form of the breakdown curves could be reproduced rather well at all residence times, when careful attention was paid to the apparatus function, the vibrational and rotational distributions, and the required convolutions.

In the present analysis we fully utilized the information contained in a given breakdown curve and treated each curve as an independent set of data. Exact counting algorithms were employed for enumeration of harmonic oscillator sums and densities of states, using frequencies coarse grained in 5 meV ($\approx 40 \text{ cm}^{-1}$) intervals. The parent ion frequencies were taken as equal to those of neutral iodobenzene [27] and several models representing transition states were considered, similar to those used in our earlier studies on chloro- and bromo-benzene [13,14]. The models employed were to change all frequencies

by a given fraction, F (model A), to change only the five halogen-dependent frequencies by a fraction F (model B), or to change only the pair of in-plane and out-of-plane halogen bending frequencies of 166 and 200 cm^{-1} by F (model C). The 654 cm^{-1} phenyl-iodine stretching frequency was always taken as the reaction coordinate.

For each transition-state model a starting value of the activation energy, E_a , and frequency change factor, F , was chosen. The corresponding rate-energy dependence was calculated using the transition-state theory expression

$$k(E^*, E_a) = W^\ddagger (E^* - E_a)/h \rho(E^*),$$

with the abovementioned exact counting algorithm for harmonic oscillator sums and density of states. The rate-energy dependence was then converted into a breakdown curve for the appropriate residence time and convoluted with the room-temperature population of vibrational levels, a classical three-dimensional rotor function and the electron energy sampling function for the NBS or Basel apparatus as required. A general non-linear multidimensional regression technique was then employed to separately fit this numerically defined function to each set of experi-

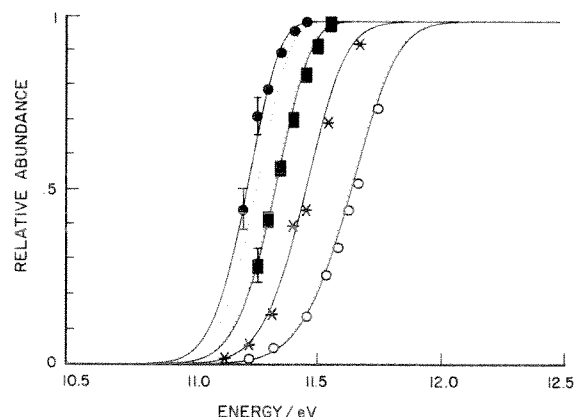


Fig. 2. The relative abundance of the C_6H_5^+ fragment ions determined in the course of this work as a function of energy and sampling time (\circ data set I, $*$ data set II, \blacksquare data set III, \bullet data set IV). The size of the symbols reflects the errors involved where no additional error bars are given. The solid lines represent the calculated results obtained by fitting each data set separately. The dotted lines correspond to our best average fit to all data sets. Note, that the two curves coincide for data set II. The 0 K threshold derived from the average fit lies at 11.015 eV.

Table 3
Best statistical fits of breakdown curves ^{a)}

Data set	Effective residence time (μs)	Crossover energy	Threshold energy ^{b)}	Equivalent 1000 K entropy of activation (cal deg^{-1})
I	1.00 ± 0.25	11.640	11.020	6.4
II	5.9 ± 0.3	11.455	11.015	6.4
III	21 ± 1	11.330	11.020	6.4
IV	57 ± 1	11.215	11.005	7.2

^{a)} Calculated using frequency variation of five halogen-dependent normal modes (model B) and treating each data set separately.

^{b)} Calculated from sum of best-fit activation energy E_a and the adiabatic ionization potential of iodobenzene 8.685 eV determined here and in ref. [24].

mental points using E_a and F as adjustable parameters.

The results of the computations are illustrated in fig. 2 for model B, (solid lines) and are summarized in table 3. For simplicity we show only the fragment ion yield data which reveal that the individual fits are quite good. Referring to the model B data in table 3 it is seen that the threshold energy, i.e. the sum of the best-fit activation energy and the ionization potential, is identical within experimental and computational error for the first three breakdown curves (data sets I, II, III). The reasons for the slightly different values obtained from data set IV are known and will be discussed below. We can conclude that there is no evidence of significant systematic error in the measurements. As previously discussed [14], we feel that this particular transition-state model allowing for changes in all the five halogen-dependent modes other than the reaction coordinate, seems physically the most reasonable. Computations with the other two transition-state models led to slightly different activation energies and equivalent activation entropies, the energy difference amounting to -0.12 eV at most and the equivalent entropy difference following in a parallel compensating manner. In particular, model A led to a best fit with a 15% decrease in all transition-state frequencies, contrary to earlier results of Baer et al. [12], who found it necessary to decrease the frequencies of the reactant. This no doubt arose from the constraint imposed by their choice of a fixed value for the activation energy.

The 5 meV coarse graining of the enumeration of oscillator states and of all of the other numerical calculations imposed limits on the precision with

which the energy and equivalent entropy parameters could be established. For example a change of 5 meV in activation energy, holding frequencies fixed, produced a rate constant change ranging from 5 to 10% over the rate constant range of interest, i.e. $\approx 10^4 - 10^6 \text{ s}^{-1}$.

For comparison, at constant activation energy, changes of ± 0.5 eu equivalent activation entropy at 1000 K led to rate constant changes of about $\pm 10\%$ in rate. Thus the best-fit equivalent entropy can be established to no better than ± 0.5 eu.

One of the uncertainties in the experimental parameters is the magnitude of the effective residence time, which is $1.0 \pm 0.25 \mu\text{s}$ for the shortest time and $57 \pm 1 \mu\text{s}$ for the longest. The effect of this on the best-fit breakdown curves and on the corre-

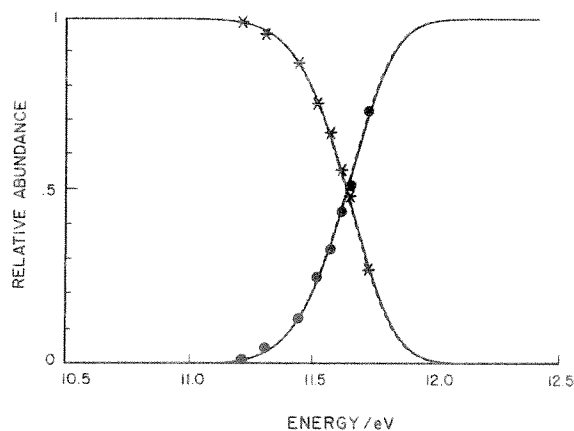


Fig. 3. Individual best fits to data set I using different values for the ion residence time of $0.75 \mu\text{s}$ (...), $1 \mu\text{s}$ (—) and $1.25 \mu\text{s}$ (- - -). Note that for these calculations model A has been used.

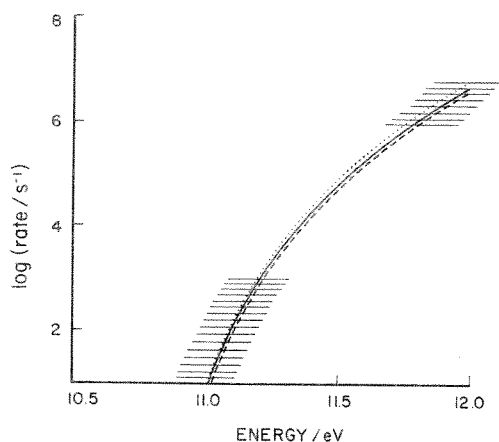


Fig. 4. The rate-energy functions corresponding to the fits presented in fig. 3. The cross-hatched regions represent extrapolated values.

sponding rate-energy functions for these two cases are shown in figs. 3–6. It is seen that the fit of the breakdown curves is hardly affected, which is not surprising, but that the resulting rate-energy dependence is slightly different. This difference in sensitivity was already noted in an earlier study [13]. In the case of the intermediate residence times ($5.9 \pm 0.3 \mu\text{s}$ and $21 \pm 1 \mu\text{s}$) the effects are even smaller than for the $57 \mu\text{s}$ case.

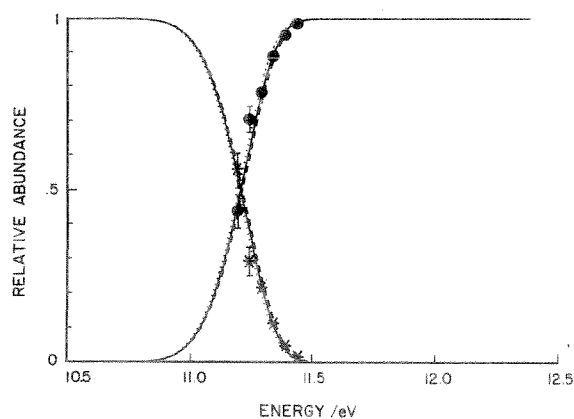


Fig. 5. Individual best fits to data set IV using different values for the parent ion flight time of $56 \mu\text{s}$ (...), $57 \mu\text{s}$ (—) and $58 \mu\text{s}$ (- - -). Note, that for these calculations model A has been used.

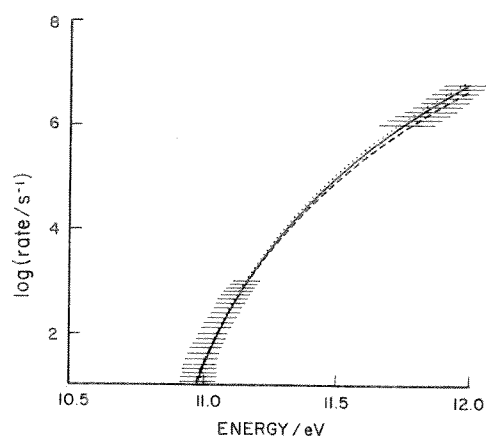


Fig. 6. The rate-energy functions corresponding to the fits presented in fig. 5. The cross-hatched regions represent extrapolated values.

3.6. The rate-energy dependence

In fig. 7 we show the rate-energy dependence determined in this study, along with the results of other

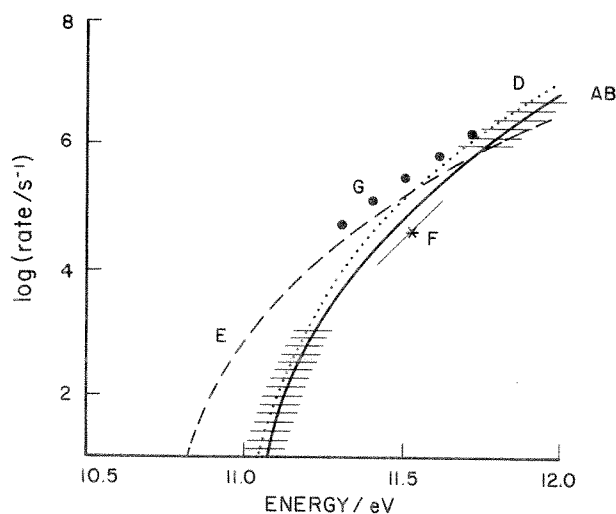


Fig. 7. Curve ABC (solid line) denotes the best individual fits to data sets I, II, and III and also our best average fit to all data sets. Curve D (...) corresponds to the best individual fit to data set IV. Curve E (- - -) represents the best-fit rate-energy dependence for data set II when all convolutions are ignored. The five points (G) were determined by Baer et al. These points were shifted 0.155 eV to higher energy to approximately account for the internal energy neglected by Baer et al. (see text). Point F and the indicated slope give the results of Pratt and Chupka. The dashed regions represent extrapolated values.

Table 4
Auxiliary thermochemistry

	Ref.
$\Delta H_{f,298}^0$ (iodobenzene)(g) = 162.2 ± 4.6 kJ mol ⁻¹	[28]
$\Delta H_{f,0}^0$ (iodobenzene)(g) = 178.2 ± 4.6 kJ mol ⁻¹	a)
$\Delta H_{f,0}^0$ (iodine)(g) = 107.25 ± 0.04 kJ mol ⁻¹	[29]
IP(iodobenzene) = 8.685 eV = 838.0 kJ/mol	this work and ref. [24]

a) Calculated from the room-temperature value and the frequencies given in ref. [27], using standard statistical mechanics methods.

workers, and with one calculated curve that illustrates the effect of neglecting the thermal energy distribution and apparatus function. The curve ABC represents the rate-energy dependences that were deduced separately from the breakdown curve data for 1.0, 5.9, and 21 μ s. They are essentially indistinguishable. The curve D represents the rate-energy dependence deduced from the 57 μ s data. It is significantly different but is derived from the least accurate data set (IV), for which lowest-energy points of the corresponding breakdown curve lie very near the onset of the photoelectron band. It is probable that because of the comparatively low energy resolution of the electron energy analyzer (80 meV fwhm gaussian) the population of ions sampled is strongly biased to ions with higher energies and higher rates than those characteristic of the nominal energy. This would lead to an overestimate of the rate, which in turn explains the different parameters obtained from this data set as compared to the other three.

If we now take as the best estimate for the activation energy and entropy the arithmetic mean of *all four* determinations given in table 3 we are led to a calculated rate-energy dependence which is essentially indistinguishable from the composite curve ABC. It is given in numerical form in table 5. A very generous estimate of the possible uncertainty in our determination is to state that the true rate-energy dependence lies in a band whose half-width is at most the interval between curves ABC and D. Since the curve ABC includes measurements on two instruments with different sources of error, this indicates that no systematic error is present, other than the one which was defined and assigned to set IV.

With this best-estimate rate-energy curve one can now examine the quality of the global fit to the orig-

inal experimental data, i.e. the breakdown curves themselves. In fig. 2 the breakdown curves calculated from this best rate-energy curve are shown as dotted lines. It is seen that the fit to all but the longest residence time data is very good, almost identical to the non-linear individual least-squares fit. For data set IV, the largest deviations are due to the two lowest energy data points which, as discussed earlier, are the most inaccurate. In effect, due to the poor Franck-Condon overlap, these data points are both biased in the energy distribution actually sampled and are of such low intensity that the statistics are relatively poor.

Table 5
Selected numerical values of the best-fit rate-energy dependence for iodobenzene fragmentation ^{a)}

Energy (eV)	Rate (s ⁻¹)
11.050 ^{b)}	3.8
11.100 ^{b)}	3.5×10^1
11.150 ^{b)}	1.6×10^2
11.200	5.4×10^2
11.250	1.5×10^3
11.300	3.8×10^3
11.350	8.6×10^3
11.400	1.8×10^4
11.450	3.5×10^4
11.500	6.6×10^4
11.550	1.2×10^5
11.600	2.0×10^5
11.650	3.4×10^5
11.700	5.4×10^5
11.750	8.5×10^5
11.800	1.3×10^6

a) Corresponding to composite curve ABC in fig. 7.

b) Refers to energies outside the experimentally accessible range.

Pratt and Chupka [19] were able to deduce a fragmentation rate at one energy and a local slope of this rate-energy dependence by analysis of a photoionization metastable. Their result is also shown in fig. 7, point F, and lies just outside the margin of error. One possible explanation for this small discrepancy is that there may be a small contribution from autoionization. This would lead to a slightly lower mean energy of the ions observed as most intense metastables. Unfortunately there is no way to correct for this.

The comparison with the data of Baer et al. [7] is not straightforward. They neglected the thermal energy and plotted the rate energy curves on a photon energy scale. Our curves, on the other hand, are plotted on an energy axis which is the total internal energy, i.e. it accounts for photon energy and the thermal energy. Baer et al. [33] have shown that the correction to their data for thermal energy can be made, to a first approximation, by shifting the energy scale by the room-temperature average thermal energy. Points G in fig. 7 are the data of Baer et al. shifted to higher energy by this amount, 0.155 eV [34]. The points agree with our data at higher energy but devi-

ate significantly at lower energy where the above approximation does not hold. To illustrate the importance of internal energy, we modeled our breakdown curves with one fictitious rate energy curve without convoluting it with the apparatus function or the thermal energy distributions. Rather good fits were obtained, but the rate energy dependence was dramatically different, see curve E in fig. 7. It is seen that this comes appreciably closer to the early result of Baer et al. [7], in particular for lower excitation energies. Clearly both apparatus and thermal distributions must be carefully taken into account or disagreements in rate energy dependences such as seen here and in similar work on chlorobenzene [13] and bromobenzene [14] will be the result.

3.7. Heat of formation of the phenyl ion

The fragmentation threshold derived in the present work, when combined with other thermochemical data leads to a 0 K heat of formation of the phenyl ion. The auxiliary thermochemical data are given in table 4 and using the 0 K fragmentation threshold

Table 6
Comparison of measurements of phenyl ion heat of formation

Parent molecule	Method	Kinetic model	$\Delta H_{f0}^0 \text{ C}_6\text{H}_5^+$ (kJ mol ⁻¹)	Ref.
C ₆ H ₅ I	coincidence	5-oscillator	1133 ± 5	this work
C ₆ H ₅ Br	coincidence	5-oscillator	1133 ± 5	[14]
C ₆ H ₅ Cl	coincidence	5-oscillator	1130 ± 5	[13,14]
C ₆ H ₅ I	photoionization metastable	loose complex, reverse Langevin	1146 ± 4	[19]
C ₆ H ₅ Br	photoionization metastable	loose complex, reverse Langevin	1146 ± 4	[19]
C ₆ H ₅ Cl	photoionization metastable	loose complex, reverse Langevin	1159	[19]
C ₆ H ₅ Br	photoionization metastable	2-oscillator	1134	[19]
C ₆ H ₅ Cl	photoionization metastable	2-oscillator	1146	[19]
C ₆ H ₅ F	fluoride ion transfer	ion-molecule reaction	1130 ± 17	[30]
—	thermal kinetics + C ₆ H ₅ radical photoionization	—	1120 ± 13	[31,32]

value of 11.015 eV we obtain a 0 K phenyl ion heat of formation of 1133 ± 5 kJ/mol. This value is compared with other independent determinations in table 6.

The first three entries in table 6 include the present results and our earlier measurements on bromobenzene and chlorobenzene [14]. All of these represent the results of a best simultaneous fit of the activation energy and of a transition-state description. The constraint on the latter was that the transition state has five halogen-dependent normal modes which are jointly adjustable as a second fitting parameter. In our earlier study on chlorobenzene we found that making all normal modes (model A) or just the in-plane, out-of-plane mode pair (model C) adjustable led to slightly different best fitting parameters. For example model A led to a value ≈ 10 kJ mol⁻¹ lower than model B. The same has been found in our present analysis on iodobenzene. Model C led to a value ≈ 6 kJ mol⁻¹ higher for chlorobenzene, but we were unable to compute a corresponding estimate for iodobenzene because of computational difficulties. Our reasoning then as now is that model B appears physically most plausible.

Pratt and Chupka [19] have recently carried out an analysis of their rate data, which is in rather close agreement with our own, using the Klots formulation of rate theory. This formulation represents in effect the loose-transition-state limit of conventional transition-state theory. The convenience of not having to assume detailed transition-state properties is offset by the uncertainty of assuming that the Langevin cross section is in fact the actual cross section for the reverse process and the additional uncertainties generated in reducing the dynamical problem to tractable form. They find that this loose-complex model leads to significantly higher values for the activation energy and resulting heat of formation of the phenyl ion. Further they found heats of formation closer to our present values when analyzing the data with a two-oscillator model, and in fact were not able to reconcile the behavior of chlorobenzene within the framework of the totally loose complex.

Thus at present, regarding the heat of formation of phenyl ion, we are left with two pictures and numbers:

(a) All three ions have a similar set of slightly loose transition states whose sum of states can be

generated by a harmonic oscillator sum, and for which the frequency pattern is plausible. These lead to a consistent value of $\approx 1131 \pm 5$ kJ mol⁻¹ for $\Delta H_{f_0}^0(\text{C}_6\text{H}_5^+)$.

(b) Bromobenzene and iodobenzene have totally loose transition states but chlorobenzene does not. Plausible reasons can be given for this qualitatively different behavior [19,35]. This leads to $\Delta H_{f_0}^0(\text{C}_6\text{H}_5^+) \approx 1146 \pm 4$ kJ mol⁻¹.

We feel, not surprisingly, that the simpler, consistent picture is more likely to be the correct one. There is some support for this from the other two independent experimental determinations. More importantly, with the availability now of reliable rate-energy data over several orders of magnitude one should be able to resolve this question by more careful measurements and analysis. The two models do not lead to exactly the same rate-energy dependence, and it should be possible to establish in an objective manner which one provides a better description of the experimental facts.

4. Conclusions

The virtually indistinguishable rate-energy dependence obtained from analysis of the various experiments indicates that no systematic error is present in the measurements. We suggest that the present results on the rate-energy dependence of iodobenzene fragmentation can serve as an absolute benchmark for calibration of future experiments. Further, the results are not dependent of the mode of ionization, i.e. direct or autoionization.

The 0 K heat of formation of the phenyl ion obtained here, 1133 ± 5 kJ mol⁻¹, is in excellent agreement with earlier results on chlorobenzene and bromobenzene fragmentation, assuming similar transition-state models. This confirms the validity of the simpler two-parameter method of data analysis developed in our previous work. The heat of formation is in closer agreement with the values obtained from less accurate independent measurements than the slightly higher value deduced from assuming a completely loose transition-state Langevin model. Further analysis or independent measurements are required to decisively settle this question.

Acknowledgement

One of us (JD) would like to thank the Schweizerischer Nationalfonds for a fellowship. The part of this work done in Basel Switzerland is part C22 of Project No. 2.622-080 of the Schweizerischer Nationalfonds zur Förderung der Wissenschaftlichen Forschung. This research was also sponsored by Ciba-Geigy S.A., Sandoz S.A., and F. Hoffmann-LaRoche & Cie. S.A., Basel, Switzerland, The partial support of this work by the US Department of Energy, Office of Environment under Contract No. 80EV 0373.000 is gratefully acknowledged. We dedicate this paper to our colleague Henry Rosenstock who died unexpectedly late this summer.

References

- [1] T. Baer, in: Gas phase ion chemistry, ed. M.T. Bowers (Academic Press, New York, 1979) ch. 5.
- [2] J.L. Holmes and J.K. Terlouw, *Org. Mass Spectrom.* 15 (1980) 383.
- [3] W.A. Chupka, in: Chemical spectroscopy and photochemistry in the vacuum ultraviolet, eds. C. Sandorfy, P.J. Ausloos and M.B. Robin (Reidel, Dordrecht, 1974).
- [4] C. Lifshitz and S. Gefen, *Intern. J. Mass Spectrom. Ion Phys.* 35 (1980) 73.
- [5] R. Stockbauer and H.M. Rosenstock, *Intern. J. Mass Spectrom. Ion Phys.* 27 (1978) 185.
- [6] J. Dannacher and J. Vogt, *Helv. Chim. Acta* 61 (1978) 361.
- [7] T. Baer, G.D. Willett, D. Smith and J.S. Phillips, *J. Chem. Phys.* 70 (1979) 4076.
- [8] H.M. Rosenstock, J. Dannacher and J.F. Liebman, *J. Rad. Phys. Chem.* 20 (1982) 7.
- [9] D. Mintz and T. Baer, *J. Chem. Phys.* 65 (1976) 2407.
- [10] J.H.D. Eland, R. Frey, A. Kuestler, H. Schulte and B. Brehm, *Intern. J. Mass Spectrom. Ion Phys.* 22 (1976) 155.
- [11] J. Dannacher, J.-P. Stadelmann and J. Vogt, unpublished results.
- [12] T. Baer, B.P. Tsai, D. Smith and P.T. Murray, *J. Chem. Phys.* 64 (1976) 2460.
- [13] H.M. Rosenstock, R.L. Stockbauer and A.C. Parr, *J. Chem. Phys.* 71 (1979) 3708.
- [14] H.M. Rosenstock, R.L. Stockbauer and A.C. Parr, *J. Chem. Phys.* 73 (1980) 773.
- [15] J.H.D. Eland and H. Schulte, *J. Chem. Phys.* 62 (1975) 3825.
- [16] H.M. Rosenstock, R.L. Stockbauer and A.C. Parr, *J. Chim. Phys.* 77 (1980) 745.
- [17] J.H.D. Eland, J. Berkowitz, H. Schulte and R. Frey, *Intern. J. Mass Spectrom. Ion Phys.* 28 (1978) 297.
- [18] H.M. Rosenstock, R.L. Stockbauer and A.C. Parr, *Intern. J. Mass Spectrom. Ion Phys.* 38 (1981) 323.
- [19] S.T. Pratt and W.A. Chupka, *Chem. Phys.* 62 (1981) 153.
- [20] Yu.L. Sergeev, M.E. Akopyan, F.I. Vilesov and V.I. Kleimenov, *Opt. Spectry.* 29 (1970) 63.
- [21] R.L. Stockbauer, *Intern. J. Mass Spectrom. Ion Phys.* 25 (1977) 89.
- [22] R. Bombach, A. Schmelzer and J.-P. Stadelmann, *Chem. Phys.* 61 (1981) 215.
- [23] R. Bombach, J. Dannacher and J.-P. Stadelman, to be published.
- [24] J. Momigny, C. Goffart and L. D'Or, *Intern. J. Mass Spectrom. Ion Phys.* 1 (1968) 53.
- [25] J.A. Sell and A. Kupperman, *Chem. Phys.* 33 (1978) 367, and references therein.
- [26] A.W. Potts, M.L. Lyas, E.P.F. Lea and G.H. Fattahallah, *J. Chem. Soc. Faraday II* 76 (1980) 556.
- [27] D.H. Whiffen, *J. Chem. Soc.* (1956) 1350.
- [28] J.B. Pedley and J. Rylance, *Sussex-N.P.L. Computer Analysed Thermochemical Data: Organic and Organometallic Compounds*, Univ. of Sussex, Sussex, UK (1977).
- [29] D.R. Stull and H.R. Prophet, eds., *JANAF thermochemical tables, NSRDS-NBS37*, 2nd Ed. (US Dept. of Commerce, June 1971).
- [30] J.L. Beauchamp, *Advan. Mass Spectrom.* 6 (1974) 717.
- [31] G.A. Chamberlain and E. Whittle, *Trans. Faraday Soc.* 67 (1971) 2077.
- [32] Yu.L. Sergeev, M.E. Ahopyan and G.I. Vilesov, *Opt. i Spektroskopiya* 32 (1972) 230.
- [33] W.A. Brand and T. Baer, *Intern. J. Mass Spectrom. Ion Phys.*, to be published.
- [34] T. Baer, private communication.
- [35] W.J. Chesnavich and M.T. Bowers, in: Gas phase ion chemistry, ed. M.T. Bowers (Academic Press, New York, 1979).